

Analysis of Individual Cosmic-Ray Proton and Helium Fluxes towards PeV Energies with DAMPE

Arshia Ruina,^{a,*} Paul Coppin,^a Andrii Kotenko,^a Peng-Xiong Ma,^b Mikhail Stolpovskiy,^a Andrii Tykhonov^a and Chuan Yue^b for the DAMPE collaboration

^a*Département de physique nucléaire et corpusculaire, University of Geneva,
Quai Ernest-Ansermet 24, 1205 Geneva, Switzerland*

^b*Key Laboratory of Dark Matter and Space Astronomy, Purple Mountain Observatory,
Chinese Academy of Sciences, Nanjing 210023, China*

E-mail: arshia.ruina@unige.ch, andrii.kotenko@unige.ch

The DArK Matter Particle Explorer (DAMPE) is a satellite-borne experiment, in operation since 2015, aimed at studying cosmic rays and high-energy gamma rays. Proton and helium are the first- and second-most abundant components in cosmic rays. Given their smaller interaction cross sections with the interstellar medium, compared to heavier nuclei, they can travel larger distances, thereby becoming important probes to cosmic-ray sources as well as acceleration and propagation mechanisms. Recently, in the DAMPE collaboration, machine learning (ML) techniques were developed and deployed to improve particle tracking and identification and correct for the calorimeter readout saturation at high energies. This work presents a direct measurement of the energy spectra of cosmic-ray protons and helium nuclei, using 84 and 81 months of data, respectively, recorded by DAMPE. Application of the above-mentioned ML techniques helps in extending the spectra to higher kinetic energies than those previously reported by DAMPE.

38th International Cosmic Ray Conference (ICRC2023)
26 July - 3 August, 2023
Nagoya, Japan



*Speaker

1. Motivation

Cosmic rays (CRs) that originate in and propagate through the Galaxy are important probes to their sources, accelerators and propagation mechanisms. Following the canonical shock acceleration mechanism, it is expected that the energy spectrum of Galactic CRs follow a power law distribution, starting from a few tens of GeV, below which energy Solar modulation effects are dominant, until the “knee” region (at around few PeV). However, recent measurements of the proton and helium CR fluxes have indicated otherwise. In particular, at rigidities ($R \sim E/Z$) of a few hundreds of GV, a hardening feature was observed for protons [1–5], helium nuclei [3, 6–9] as well as heavier nuclei by several experiments. Moreover, improvements in measurements at higher energies have also found hints of a softening feature at rigidities of about 10 TV [7, 10] which were later confirmed by other experiments that studied CR protons [4, 5] and helium [6, 9]. This softening appears at energies lower than the conventional “knee” on the all-particle spectrum [11] as measured by numerous air-shower experiments, where measurements for individual elemental compositions have relatively large uncertainties. Most recently, preliminary results on the proton plus helium spectrum as measured by the HAWC experiment [12] showed a softening feature at an energy of about 30 TeV, which was later confirmed by DAMPE [13].

These deviations in the CR spectrum and recent developments in modelling [14] motivate a further investigation into the measurements of CR fluxes, especially for proton and helium nuclei, which are the two most abundant components of cosmic rays. This will help to understand better the underlying mechanisms behind CR acceleration and propagation in the interstellar medium. In this contribution, the updated spectra for protons and helium nuclei are presented, up to 120 TeV kinetic energy (equivalent to 30 TeV/nucleon for helium) and using 84 and 81 months of data from the DAMPE experiment, respectively. Deep-learning techniques that were recently developed in the collaboration [15, 16] have been deployed in both the analyses. Extension of the spectra to higher energies is currently in progress and beyond the scope of this proceeding.

2. The DAMPE Experiment

The DARK Matter Particle Explorer (DAMPE) mission [17] is a satellite-borne detector for cosmic rays and gamma rays, that was launched in December 2015 from the Jiuquan Satellite Launch Center in China. It follows a Sun-synchronous orbit around the Earth at an altitude of about 500 km. The scientific goals of DAMPE include understanding the mechanisms of acceleration of cosmic-ray particles in astrophysical sources, and their propagation in the Galaxy, as well as studying gamma-ray emissions from Galactic and extra-Galactic sources and probing the nature of dark matter through the precise measurements of cosmic-ray particle spectra. DAMPE can measure electrons and gamma rays in the energy range ~ 5 GeV to ~ 10 TeV, while for protons and heavier ions, the energy range extends from ~ 50 GeV to several hundreds of TeV. The detector system (see figure 1) comprises a plastic scintillator detector (PSD) for charge measurement, which also acts as an anticoincidence detector, a silicon-tungsten tracker-converter (STK) for particle track measurement and photon conversion, which also provides information on the particle charge, and a bismuth germanium oxide (BGO) calorimeter for energy measurement (depth of $1.6 \lambda_I$ or $32 X_0$),

which also provides the trigger and helps in particle identification and track reconstruction, and a neutron detector (NUD) that further aids in lepton-hadron separation.

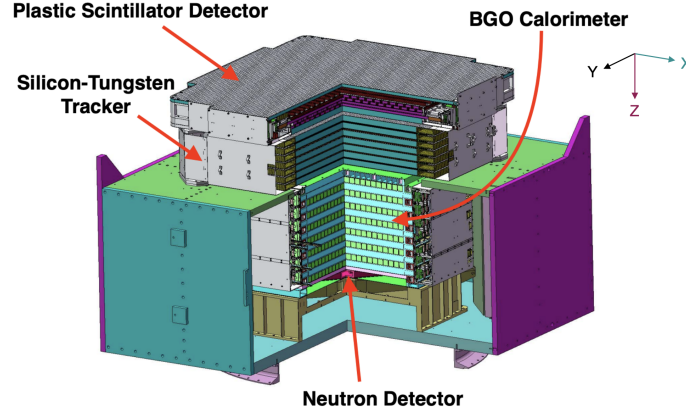


Figure 1: A schematic view of DAMPE and its sub-detectors.

3. The Proton and Helium Analyses

The differential flux Φ for a cosmic-ray particle species in a given energy range $[E, E + \Delta E]$ can be expressed as

$$\Phi(E, E + \Delta E) = \frac{N(E, E + \Delta E)}{\Delta T A_{\text{eff}} \Delta E} \quad (1)$$

where $N(E, E + \Delta E)$ is the number of candidate particles that were observed in that energy range and can also be expressed as $N_{\text{observed}} - N_{\text{background}}$, ΔT is the effective observation or data collection time (referred to as the live-time) of the detector, A_{eff} is the effective acceptance and ΔE is the width of the energy interval. Two independent analyses were carried out for measuring the proton and the helium fluxes which are presented in the following sections. Unless otherwise mentioned, both analyses closely follow the same procedures.

Flight data. For the CR proton and helium flux measurements, 84 and 81 months of data are used that amounted to a total of 13.03 and 12.57 billion events, respectively. After accounting for various detector dead-times, a total livetime of 1.63×10^8 and 1.58×10^8 seconds is obtained for proton and helium, respectively.

Pre-selection Cuts. To ensure that only well-reconstructed and interesting events are used in the analyses, a set of pre-selection cuts are applied on the data. (a) Only events that pass the High Energy Trigger (HET) are used in the analyses. The HET requires that the energy deposited in the first three layers of the BGO calorimeter is higher than 10 times the proton minimum ionizing particle (MIP) energy (about 23 MeV in one layer) and that in the fourth layer is higher than twice the proton MIP energy. (b) The total energy deposited in the first two layers of the BGO calorimeter is required to be smaller than that in the third and fourth layers, ensuring that the particle shower starts at the top of the calorimeter. (c) The geomagnetic rigidity cutoff effect is accounted for by rejecting events with total deposited energy less than 20 GeV. (d) Events in the South Atlantic Anomaly region are not recorded. (e) Side-entering (in the calorimeter) events are discarded by

requiring that the energy recorded in a layer is less than 35% of the total energy. It is also required that (f) the reconstructed shower vector is within ± 280 mm from the center of the top and bottom layers of the calorimeter and that (g) for the top layers the bars with maximum deposited energy are not on the edges.

Simulations. Monte Carlo (MC) simulated data are also used to evaluate the performance of the analysis. For both CR flux measurements, 0.5 billion helium and 11 billion proton events are simulated in the energy range 10 GeV to 1 PeV. The FTFP-BERT (FriTioF-BERTini cascade) model for hadronic interactions provided by the GEANT Toolkit version 4.10.5 [18–20] was used. CRMC-Geant4 interface [21, 22] was used to describe interactions with EPOSLHC model at very high energies, which better describes particle interactions in this energy regime. Also, Monte Carlo samples using FLUKA were produced to estimate hadronic interaction simulation uncertainty. All simulated events are reconstructed and the triggering and pre-selection cuts applied are identical to those on the flight data.

Track selection. A Convolutional Neural Network (CNN)-based model [16] predicts the particle track direction and its closest hits in the STK layers. The requirements imposed on this track are (a) Fiducial containment: the reconstructed track direction from BGO calorimeter should pass through the top and bottom layers of the calorimeter and (b) Match with PSD hit: the reconstructed track direction from the STK should coincide with at least one hit in the PSD.

Charge Selection and Background Subtraction. First, a set of calibrations and corrections are made to the signals from both the sub-detectors [23–31]. For the MC data to better match the flight, a smearing correction is introduced for the PSD and the STK signals. Furthermore, the energy measured from the BGO calorimeter is corrected for saturation effects using a new CNN-based algorithm [15].

For both flux measurements, the particle charge information from both, the PSD as well as the STK are used. The PSD charge is defined as an average over non-zero and consistent signals from the 4 sublayers in the PSD. For the STK, an average signal value is defined by starting from the first STK layer, progressively taking the average over non-zero signals, as long as the signal of the next layer is consistent with the previous average, and stopping the procedure when more than one inconsistent signals are encountered.

For the separation of proton and helium from other particles, we define a so-called “combined” charge and for each analysis we use a slightly different definition. The combined charge is calculated by providing different charge estimates depending on the event’s vertex probability, which is the classifier’s prediction from [16], that gives the probability of inelastic interactions taking place within the PSD or before the primary particle enters the STK. When vertex has a “good” value, implying low probability of inelastic interactions, a normalized charge estimate from STK is taken for the proton analysis, while the geometric average of PSD and STK charge estimates is used for the helium analysis. For a “bad” value, it equals to charge estimate from PSD only.

Protons have two major sources of background: electrons and helium. Hadronic and electromagnetic showers are very different in nature and significantly differ in lateral and longitudinal profiles, so we define a variable that encapsulates these differences to separate protons from electrons. Residual electron background is negligible. Further, we use a fixed window cut on the combined charge to remove the helium background. We manage to keep background smaller than 2% up to 100TeV.

For the helium analysis, protons are the dominant background. As such, an additional selection criterium is imposed to reject the proton background by requiring that the average signal from the first two hits in the STK be larger than 100 ADC (the proton signal lies at around 60 ADC). Furthermore, to ensure a consistency in the charges measured by the two orthogonal layers of the PSD, it is also required that the absolute value of the charge difference between the two be <1 .

The helium signal region is defined as energy-dependent windows around the helium peaks in each energy interval as shown by the dashed vertical lines in figure 2.

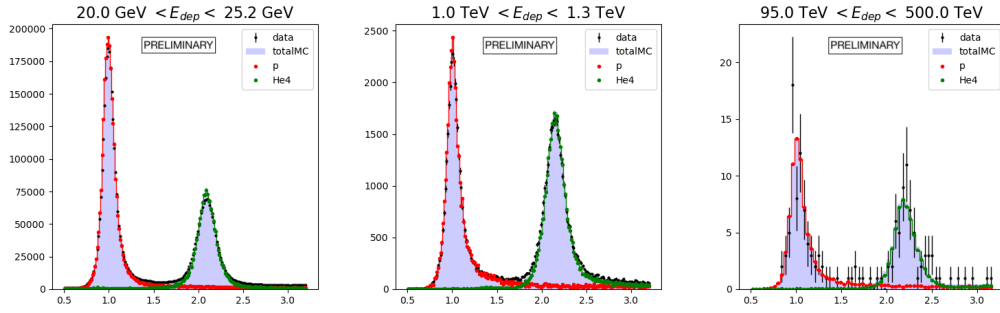


Figure 2: Proton analysis: Template fits to the combined charge distributions in three deposit energy intervals.

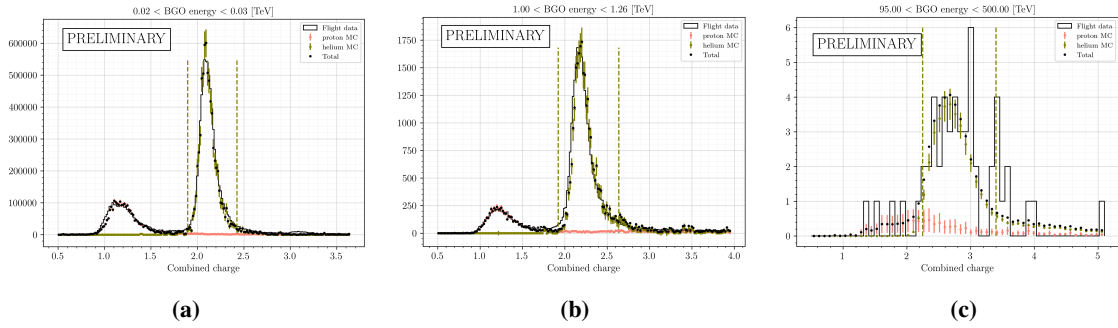


Figure 3: Helium analysis: Template fits to the combined charge distributions, after the application of the selection cuts (incl. proton rejection), in various deposit-energy intervals.

Acceptance and Unfolding. The effective acceptance, A_{eff} , is computed as $A_{\text{eff},i} = A_{\text{gen}} \times \frac{N_{\text{pass},i}}{N_{\text{gen},i}}$ for the i -th interval in incident energy, where, A_{gen} is the geometrical factor of the MC event generator sphere and $N_{\text{pass},i}$ is the number of events in MC data that passed the selection cuts and $N_{\text{gen},i}$ are the total number of MC events generated. The final effective acceptances for the proton and helium flux measurements are shown in figures 4. The slight wiggles in the helium acceptance are caused by the track selections and are currently under investigation. Following [32], an unfolding procedure is employed to convert the measured energy of the particles into their kinetic (or incident) energy.

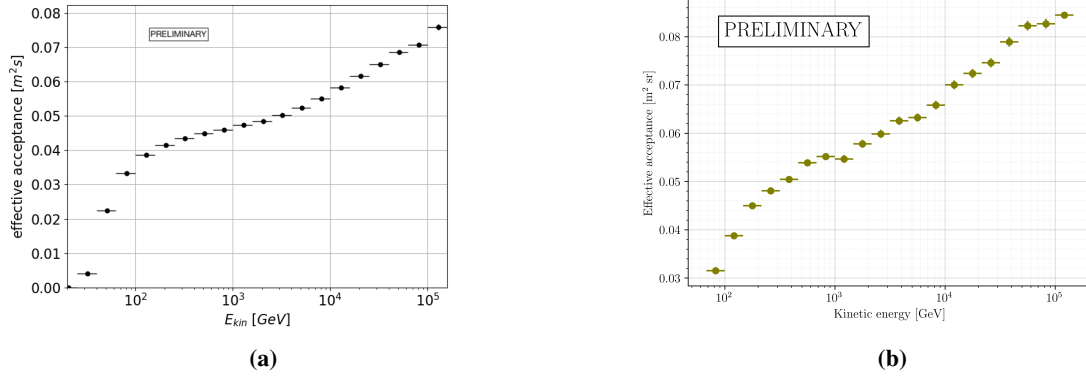


Figure 4: Effective acceptances for (a) protons and (b) helium ions.

4. Results

Statistical uncertainties originate from the Poissonian fluctuations in the observed data which increase with energies. They are very similar for both the fluxes and are around 0.05% at 100 GeV incident energies and go up to 6-8% at 100 TeV. Systematic uncertainties for both analyses are below 10% across all energies with the dominant sources being the detector trigger and charge selection efficiencies.

In addition to using the Geant4 MC data, the analyses were also performed with MC data generated using the FLUKA hadronic model. The resulting difference in the flux is taken as the hadronic systematic uncertainty, that reach a maximum of 11% and 18% for the proton and helium fluxes, respectively. Uncertainties from hadronic models, arising mainly from discrepancies in cross sections in the MC generators, constitute a dominant source of systematics and is an often-encountered challenge in space-based calorimetric particle detectors. In-depth studies are currently under way in the collaboration to better account for them in the future [33].

The measured CR proton and helium fluxes are shown in figures 5, together with statistical and systematic uncertainties, and in comparison to results from other experiments. Both the fluxes are in good agreement with DAMPE's previous results from 2019 for protons [4] and from 2021 for helium [6].

5. Conclusions

In this study, we present updated measurements of proton and helium fluxes, incorporating additional flight data and employing advanced analysis techniques. Notably, we introduce the utilization of ML STK tracking for flux measurements, enhancing precision of charge definition, background estimation and acceptance. Our findings confirm the presence of spectral hardening and softening in both helium and proton fluxes. To analyze the spectra, we perform a spectral fitting with nuisance parameters, as detailed in [4], resulting in updated break positions. The results of the fit, displayed in figures 6, demonstrate that the charge-dependence of cosmic rays is favored over mass-dependence, as evidenced by the improved alignment of the break energy positions in the rigidity plots. This achievement marks a significant advancement, and we are currently finalizing

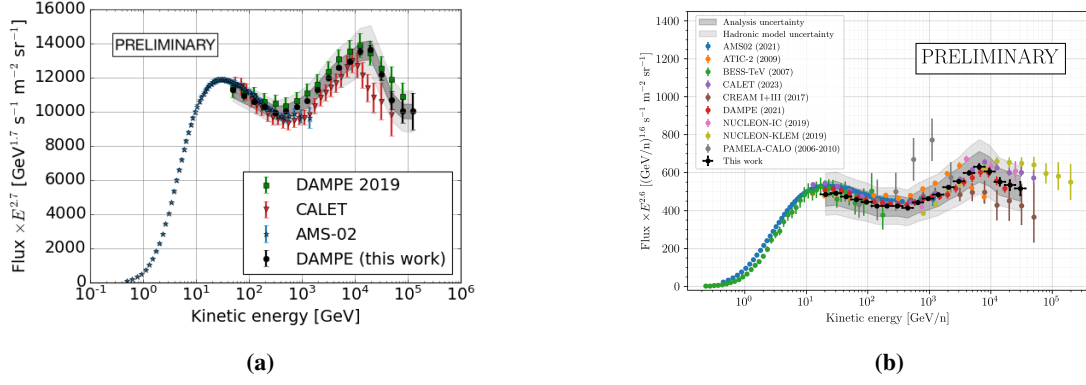


Figure 5: (a) The proton spectrum, as measured in this work, weighted with $E^{2.7}$, as a function of kinetic energy, in comparison with results from the AMS [34] and CALET [5]. (b) The helium spectrum, as measured in this work, weighted with $E^{2.6}$, as a function of kinetic energy per nucleon, in comparison with results from other experiments [6, 35–42]. The inner and outer shaded bands denote the systematic uncertainties from the analysis and the total systematic uncertainties, including those from hadronic models, respectively.

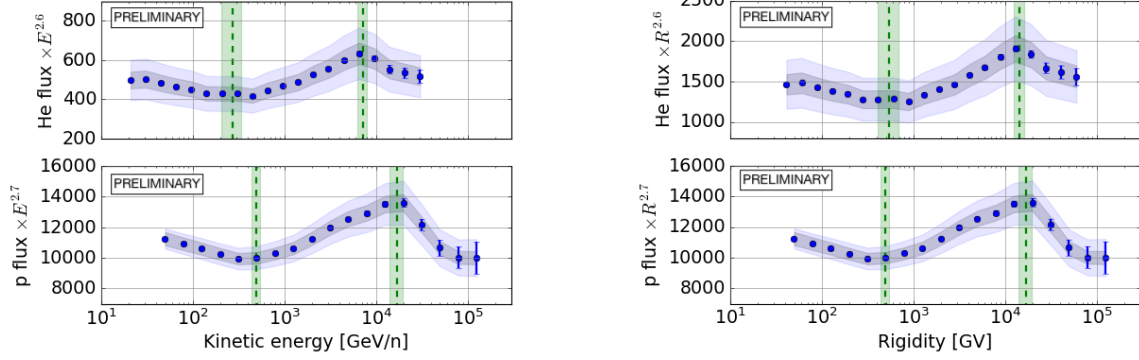


Figure 6: Helium (top plots) and proton (bottom plots) fluxes as function of kinetic energy per nucleon (left plots) and rigidity (right plots). Positions of the hardening and softening breaks, as obtained from the spectral fitting with nuisance parameters, are shown with the green vertical dashed lines, where the green vertical bands correspond to uncertainties. Statistical and systematical uncertainties on the flux points are the same as in figures 5. y-axis units of left plots are same as in figures 5 while y-axis units of right plots are $(\text{GV})^{1.6} \text{ s}^{-1} \text{ m}^{-2} \text{ sr}^{-1}$ for the helium flux and $(\text{GV})^{1.7} \text{ s}^{-1} \text{ m}^{-2} \text{ sr}^{-1}$ for the proton flux.

the analysis to provide a comprehensive estimation of the significance for these intriguing spectral features.

Acknowledgements

The DAMPE mission was funded by the strategic priority science and technology projects in space science of Chinese Academy of Sciences (CAS). In China, the data analysis was supported by the National Key Research and Development Program of China (No. 2022YFF0503302) and the National Natural Science Foundation of China (Nos. 12103094, 12220101003, 11921003, 11903084, 12003076 and 12022503), the CAS Project for Young Scientists in Basic Research (No. YSBR061), the Youth Innovation Promotion Association of CAS, the Young Elite Scientists

Sponsorship Program by CAST (No. YESS20220197), and the Program for Innovative Talents and Entrepreneur in Jiangsu. In Europe, the activities and data analysis are supported by the Swiss National Science Foundation (SNSF), Switzerland, the National Institute for Nuclear Physics (INFN), Italy, and the European Research Council (ERC) under the European Union's Horizon 2020 research and innovation programme (No. 851103).

References

- [1] G. H. Choi et al., *Astrophys. J.* **940** (November, 2022) 107.
- [2] O. Adriani et al., *Science* **332** (2011) 69–72.
- [3] M. Aguilar et al., *Phys. Rep.* **894** (2021) 1–116.
- [4] Q. An et al., *Sc. Adv.* **5** (2019) 9.
- [5] O. Adriani et al., *Phys. Rev. Lett.* **129** (2022).
- [6] F. Alemanno et al., *Phys. Rev. Lett.* **126** (May, 2021).
- [7] Y. S. Yoon et al., *Astrophys. J.* **839** (April, 2017) 5.
- [8] O. Adriani et al., *Adv. Space Res.* **51** (2013) 219–226.
- [9] O. Adriani et al., *Phys. Rev. Lett.* **130** (2023).
- [10] E. Atkin et al., *JETP Lett.* **108** (2018) 5–12.
- [11] J. R. Hörandel, *J. Phys.: Conf. Ser.* **47** (2006).
- [12] A. U. Abeysekara et al., *PoS ICRC 374* (2021).
- [13] F. Alemanno et al., *arXiv:2304.00137 pre-print* (2023).
- [14] C. Yue et al., *Front. Phys.* **15** (December, 2019).
- [15] M. Stolpovskiy et al., *JINST* **17** (June, 2022) P06031.
- [16] A. Tykhonov et al., *Astropart. Phys.* **146** (2023) 102795.
- [17] J. Chang et al., *Astropart. Phys.* **95** (2017) 6–24.
- [18] S. Agostinelli et al., *Nucl. Instr. Meth. Phys. Res. A* **506** (2003) 250–303.
- [19] J. Allison et al., *IEEE Trans. Nuc. Sci.* **53** (2006) 270–278.
- [20] J. Allison et al., *Nucl. Instr. Meth. Phys. Res. A* **835** (2016) 186–225.
- [21] R. Ulrich et al.
- [22] A. Tykhonov et al., *PoS(ICRC2019)143* (2019).
- [23] G. Ambrosi et al., *Astropart. Phys.* **106** (2019) 18–34.
- [24] P.-X. Ma et al., *Res. Astron. Astrophys.* **19** (June, 2019) 082.
- [25] M. Ding et al., *Res. Astron. Astrophys.* **19** (March, 2019) 047.
- [26] A. Tykhonov et al., *Nucl. Instr. Meth. Phys. Res. A* **924** (2019) 309–315.
- [27] C. Perrina et al., *PoS(ICRC2021)084* (2021).
- [28] E. Catanzani et al., *J. Phys.: Conf. Ser.* **2374** (November, 2022) 012067.
- [29] A. Tykhonov et al., *Nucl. Instr. Meth. Phys. Res. A* **893** (2018) 43–56.
- [30] S. Vitillo and V. Gallo, *PoS(ICRC2021)240* (2017).
- [31] A. Ruina et al., *PoS(ICRC2021)083* (2021).
- [32] G. D'Agostini, *Nucl. Instr. Meth. Phys. Res. A* **362** (1995) 487–498.
- [33] P. Coppin et al., *PoS(ICRC2023)XXX* (2023).
- [34] M. Aguilar et al., *Phys. Rev. Lett.* **114** (Apr, 2015) 171103.
- [35] M. Aguilar et al., *Phys. Rep.* **894** (2021) 1–116.
- [36] A. D. Panov et al., *Bull. Russ. Acad. Sci. Phys.* **73** (2009) 564–567.
- [37] Y. Shikaze et al., *Astropart. Phys.* **28** (2007) 154–167.
- [38] O. Adriani et al., *Phys. Rev. Lett.* **130** (April, 2023) 171002.
- [39] Y. S. Yoon et al., *Astrophys. J.* **839** (April, 2017) 5.
- [40] V. Grebenyuk et al., *Adv. Space Res.* **64** (2019) 2546–2558.
- [41] V. Grebenyuk et al., *Adv. Space Res.* **64** (2019) 2559–2563.
- [42] O. Adriani et al., *Adv. Space Res.* **51** (2013) 219–226.